Unifying approach to left-handed material design

Jiangfeng Zhou

Department of Electrical and Computer Engineering and Microelectronics Research Center, Iowa State University, Ames, Iowa 50011

Eleftherios N. Economon

Institute of Electronic Structure and Laser—FORTH, and Department of Physics, University of Crete, Greece

Thomas Koschny and Costas M. Soukoulis

Ames Laboratory and Department of Physics and Astronomy, Iowa State University, Ames, Iowa 50011 and Institute of Electronic Structure and Laser—FORTH, and Department of Materials Science and Technology, University of Crete, Greece

Received July 19, 2006; accepted September 2, 2006;
posted September 29, 2006 (Doc. ID 73166); published November 22, 2006

We show that equivalent circuits offer a qualitative and even quantitative simple explanation for the behavior of various types of left-handed (or negative-index) metamaterials. This allows us to optimize design features and parameters while avoiding trial and error simulations or fabrications. In particular, we apply this unifying circuit approach in accounting for the features and in optimizing the structure employing parallel metallic bars on the two sides of a dielectric film. © 2006 Optical Society of America

OCIS codes: 160.4760, 260.5740.

Left-handed materials exhibit a negative permeability, μ, and permittivity, ϵ, over a common frequency range.[1] Negative permeability is the result of a strong resonance response to an external magnetic field; negative permittivity can appear by either a plasmonic or a resonance response (or both) to an external electric field. Negative μ and negative ϵ lead to a negative index of refraction, n, and to a left-handed triad of $\vec{k}, \vec{E}, \vec{H}$; hence the names "negative-index materials" (NIMs) or "left-handed materials." Pendry *et al.*[2,3] suggested a double metallic split-ring resonator (SRR) design for negative μ and a parallel metallic wire periodic structure for an adjustable plasmonic response. Several variations of the initial design have been studied; among them, a single-ring resonator with several cuts has been proved capable of reaching negative μ at a higher frequency[4]; in Fig. 1(a) a two-cut single ring is shown schematically. This, by continuous transformation, can be reduced to a pair of carefully aligned metal bars separated by a dielectric spacer of thickness t_s.[5,6] In Figs. 1(b) and 1(c) the view in the $(\vec{E},\vec{k})$ and $(\vec{E},\vec{H})$ planes of this structure is shown together with the directions of $\vec{k}, \vec{E}, \vec{H}$ of the incoming electromagnetic field.

The design shown in Figs. 1(b) and 1(c), besides its simplicity, has distinct advantages over conventional SRRs. The incident electromagnetic wave is normal to the structure, as shown in Fig. 1(c), which enables us to build NIMs with only one layer of sample and to achieve a relatively strong response. Conventional SRRs, although they exhibit magnetic resonance that may produce negative μ, fail to give negative ϵ at the same frequency range, and hence by themselves they are incapable of producing NIMs. An extra continuous wire is needed to obtain negative ϵ via a plasmonic response.[2,7] In contrast, the pair of parallel metallic plates is expected to exhibit not only a magnetic resonance [Fig. 2(c), antisymmetric mode] but also an electric resonance as well [symmetric mode], properly located in frequency by adjusting the length, l, of the pair.

The simulations were done with the CST Microwave Studio (Computer Simulation Technology GmbH, Darmstadt, Germany) by using the lossy metal model for copper with a conductivity $\sigma = 5.8 \times 10^7$ for a single unit cell with a periodic boundary in the $(\vec{E},\vec{H})$ plane; field distribution and scattering amplitudes have been calculated. The ϵ and μ in Fig. 5 below were obtained by a retrieval procedure.[8] At the magnetic resonance the two plates sustain antiparallel currents, producing a magnetic field $\vec{B}$ confined mainly in the space between the plates and di-

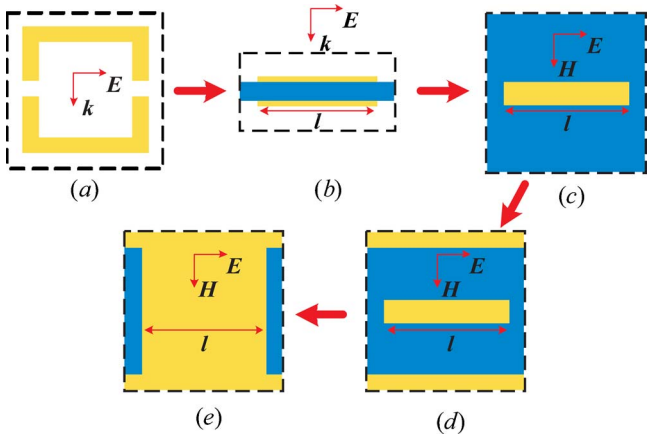

Fig. 1. (Color online) The two-cut single metallic SRR (a) can be transformed to a pair of parallel metallic bars separated by a dielectric; (b) view in $(\vec{E},\vec{k})$ plane; (c) view in $(\vec{E},\vec{H})$ plane. Adding continuous wires results in design (d) [view in $(\vec{E},\vec{H})$ plane], which can be modified to (e) a fully connected one on both sides of the thin dielectric board. The dashed squares define unit cells with dimensions a_x (parallel to $\vec{H}$), a_y (parallel to $\vec{E}$), and a_z (parallel to $\vec{k}$).

0146-9592/06/243620-3/$15.00

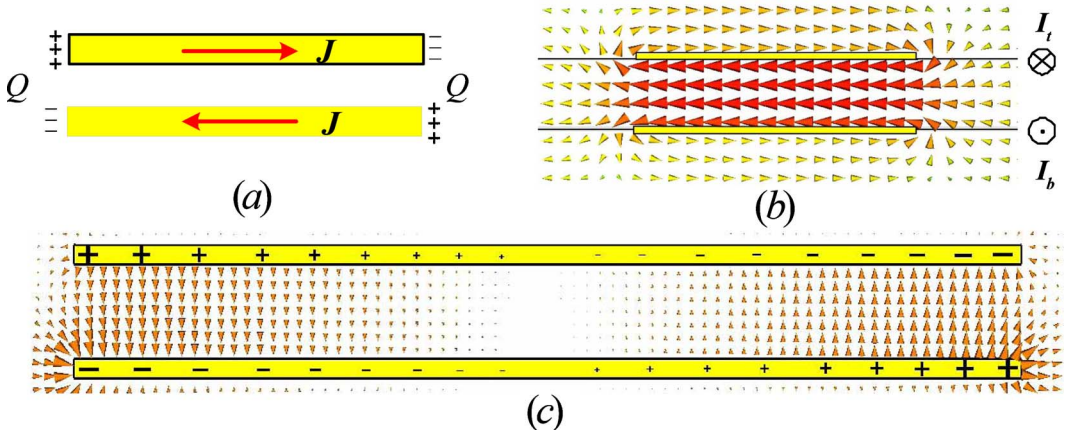

Fig. 2. (Color online) At magnetic resonance the currents (a) [in the $(\vec{E},\vec{k})$ plane, view in the $\vec{H}$ direction], the magnetic field (b) [in the $(\vec{H},\vec{k})$ plane] and the electric field (c) [in the $(\vec{E},\vec{k})$ plane] are shown. Sizes of the cones show the intensity of (b) magnetic field $\vec{H}$ and (c) electric field $\vec{E}$ on a logarithmic scale.

rected opposite to that shown in Fig. 1(c); the electric field, because of the opposite charges accumulated at the ends of the two plates, is expected to be confined within the space between the plates and near the end points. Indeed, detailed simulations, shown in Fig. 2(c), confirm this picture.

At the electric resonance the currents at the two bars are parallel (symmetric mode); the magnetic field lines go around both bars, while the electric field is confined mostly in the space between the nearest-neighbor edges of the two pairs of bars belonging to consecutive unit cells.

The field and current configurations for both the antisymmetric and the symmetric mode can be accounted for by equivalent R, C, L circuits as shown in Fig. 3 (in which for simplicity the resistor elements have been omitted). Near the magnetic resonance frequency, for a current configuration as in Fig. 3(c), the magnetic field is between the two plates, and it is, to a good approximation, uniform [Fig. 2(b)]. Hence the total inductance L, as calculated by the magnetic field energy, is $L=2L_m\simeq\mu(t_s/w)l$, where l is the length of the wire, t_s is the thickness of the dielectric spacer, and w is the width of the wire.

Notice that at telecommunication or optical frequencies, where the linear dimensions are in the tens or hundreds of nanometers, the kinetic energy of the drifting electrons makes a contribution comparable or larger than the magnetic energy. Hence another additional inductance must be added to the right-hand side of the equation for L.[4]

Each capacitance C_m must be given by a formula of the type $C_m=\epsilon w l'/t_s$, where, by inspection of Fig. 2(c), $l'=c_1 l$ with the numerical factor c_1 in the range $0.2\leq c_1\leq 0.3$. The capacitance C_e can be approximated by that of two parallel wires of radius t_m and length w at a distance b apart, $C_e=\pi\epsilon w/\ln(b/t_m)$, where t_m is the thickness of each metallic bar and b is the separation of neighboring pairs; see Figs. 3(a) and 3(b) ($b=a_y-l$). The magnetic resonance frequency, ω_m, is obtained by equating the impedance Z (of L_m and C_e in parallel) with minus the impedence $-i/C_m\omega$ of the capacitance C_m.

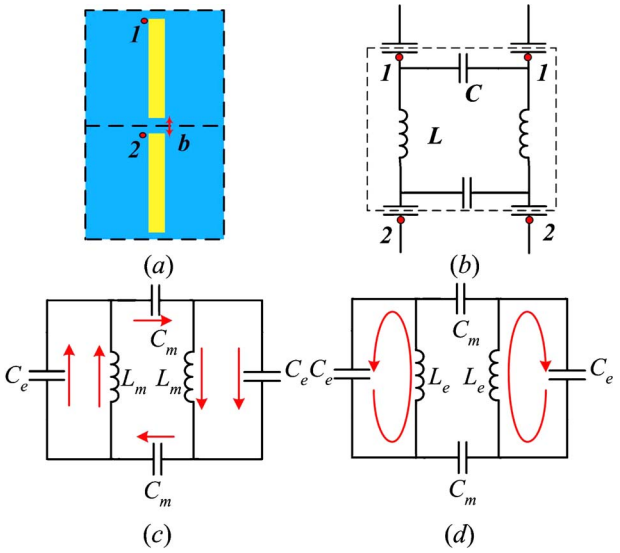

Fig. 3. (Color online) Current distribution of the design with two parallel metallic bars (a) [view in plane, one parallel plate is behind the other] can be accounted for by (b) the equivalent circuit, which, since points 1 and 2 are equivalent because of the periodicity, reduces to circuits (c) and (d) for the magnetic and electric resonances, respectively.

Since $Z=iL_m\omega/(1-L_mC_e\omega^2)$, we obtain $\omega_m=1/\sqrt{L_m(C_m+C_e)}\simeq 1/\sqrt{L_mC_m}$. The last relation follows because, for the values we have used ($l=7$ mm, $w=1$ mm, $t_s=0.254$ mm, $t_m=10$ μm, and $b=0.3$ mm), $C_e\simeq 0.1C_m$. Combining the equations for L and C_m, we find that

$$f_m=\frac{\omega_m}{2\pi}=\frac{1}{2\pi l\sqrt{\epsilon\mu}\sqrt{c_1/2}}=\frac{1}{2\pi\sqrt{c_1\epsilon_r/2}}\frac{c}{l}, \qquad (1)$$

where $\epsilon_r=2.53$ is the reduced dielectric constant of the dielectric, $\epsilon_r=\epsilon/\epsilon_0$. Equation (1) shows that f_m is a linear function of only $1/l$, which agrees very well with our detailed simulation results.

For frequencies near the electric resonance, because of the mirror symmetry in Fig. 3(d), there is no current passing through the capacitances C_m. As a

result the electric resonance frequency f_e is given by $f_e = 1/(2\pi\sqrt{C_e L_e})$, where L_e is expected to be of the form $(\mu/\pi)g(w/l)$, where $g(x)$ is a function that for $x \to 0$ behaves as $-\ln(x)$.

We point out that f_e is a rather sensitive function of the small distance b, because C_e depends on b, while L_e is practically independent of b. Indeed the ratios $f_e(2b)/f_e(b)$ and $f_e(3b)/f_e(b)$ for $b = 0.1$ mm according to the equation for C_e and equation for f_e are, respectively, 1.14 and 1.215, in good agreement with the simulation results in Fig. 4 (1.13 and 1.21, respectively); the dependence of both f_m and f_e on $a_y/l = 1 + b/l$ is shown in Fig. 4.

Figure 4 in combination with Fig. 5 suggests the optimum design parameters for making the two-bar scheme produce negative index n: one has to avoid the crossing region where, essentially, to a considerable degree the two resonances cancel each other. Since the electric resonance is much stronger and hence much wider, we have to bring the magnetic resonance within the negative region of ϵ; i.e., we must have f_e lower than f_m as in Fig. 5(b), rather than the other way around; i.e., we must have

$$\left(\frac{f_e}{f_m}\right)^2 = \frac{L_m}{L_e}\left(1 + \frac{C_m}{C_e}\right) < 1. \qquad (2)$$

This can be achieved by increasing C_e, either by decreasing b or by increasing at the ends of each bar the width w, choosing a double T shape for each bar.[9]

Still another possibility to make the negative ϵ region wider (and more negative) is to add continuous metallic wires as in Fig. 1(d), which produce a plasmonic response.[5] Adjusting the width of these wires can make their effective plasma frequency f_p larger than the frequency f_1 at which the continuous curve in Fig. 5(b) crosses the axis ($f_1 \simeq 16$ GHz).

Finally, the width of the bars, w, can increase until the bars join the infinite wires, thus producing a continuous connected network that can be constructed

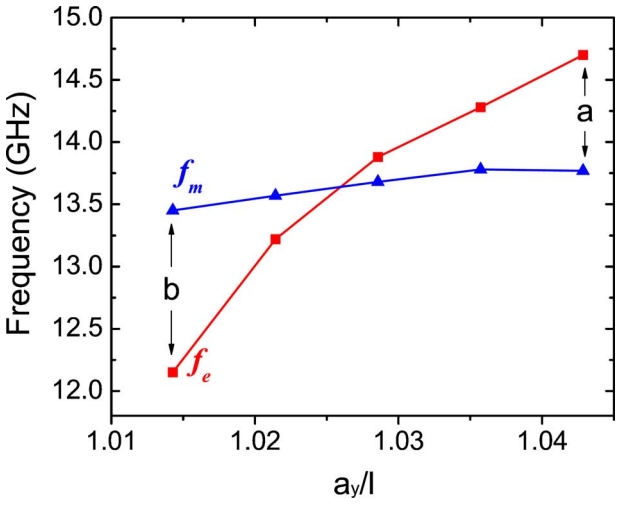

Fig. 4. (Color online) Magnetic resonant frequency f_m crossover with electrical resonant f_e as $a_y/l = 1 + b/l$ varies between 7.1 mm and 7.3 mm; $a_x = 20$ mm.

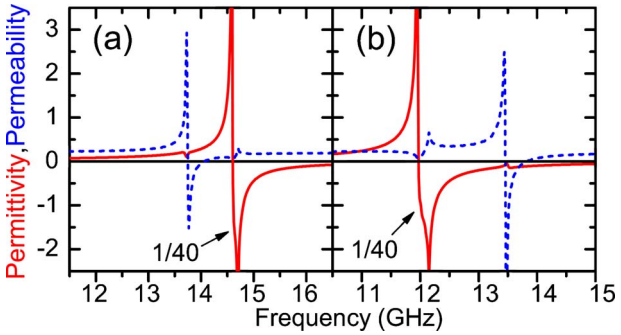

Fig. 5. (Color online) Retrieved ϵ_{eff} (solid curves) and μ_{eff} (dotted curves) for two cut wires. (a) and (b) correspond to points a ($a_y = 7.3$ mm, $a_x = 20$ mm) and b ($a_y = 7.1$ mm, $a_x = 20$ mm) in Fig. 4. Notice that both responses are Lorentz-like.

by opening periodically placed rectangular holes in uniform metallic films covering both sides of a dielectric sheet.[10–12]

In this Letter we have shown that L, C equivalent circuits can account for the electromagnetic properties of various negative-index artificial metamaterials (NIMs), even at a quantitative level; furthermore, this simple unifying circuit approach offers clear guidance in adjusting the design and optimizing the parameters for existing and possible future NIMs.

We gratefully acknowledge the support of Ames Laboratory (operated by Iowa State University under contract W-7405-Eng-82), the Air Force Office of Scientific Research under Multidisciplinary University Research Initiative grant FA9550-06-1-0337, EU projects METAMORPHOSE, PHOREMOST, and LSHG-CT-2003-503259, and Defense Advanced Research Projects Agency contract HR0011-05-C-0068.

References

1. V. Veselago, Sov. Phys. Usp. **10**, 509 (1968).
2. J. Pendry, A. Holden, W. Stewart, and I. Youngs, Phys. Rev. Lett. **76**, 4773 (1996).
3. J. Pendry, A. Holden, D. Robbins, and W. Stewart, IEEE Trans. Microwave Theory Tech. **47**, 2075 (1999).
4. J. Zhou, T. Koschny, M. Kafesaki, E. N. Economou, J. B. Pendry, and C. M. Soukoulis, Phys. Rev. Lett. **95**, 223902 (2005).
5. J. Zhou, L. Zhang, G. Tuttle, T. Koschny, and C. M. Soukoulis, Phys. Rev. B **73**, 041101 (2006).
6. V. M. Shalaev, W. S. Cai, U. K. Chettiar, H. K. Yuan, A. K. Sarychev, V. P. Drachev, and A. V. Kildishev, Opt. Lett. **30**, 3356 (2005).
7. D. Smith, W. Padilla, D. Vier, S. Nemat-Nasser, and S. Schultz, Phys. Rev. Lett. **84**, 4184 (2000).
8. D. R. Smith, S. Schultz, P. Markos, and C. M. Soukoulis, Phys. Rev. B **65**, 195104 (2002).
9. J. Zhou, T. Koschny, L. Zhang, G. Tuttle, and C. M. Soukoulis, Appl. Phys. Lett. **88**, 221103 (2006).
10. G. Dolling, C. Enkrich, M. Wegener, C. M. Soukoulis, and S. Linden, Science **312**, 892 (2006).
11. S. Zhang, W. Fan, B. K. Minhas, A. Frauenglass, K. J. Malloy, and S. R. J. Brueck, Phys. Rev. Lett. **94**, 037402 (2005).
12. S. Zhang, W. Fan, N. C. Panoiu, K. J. Malloy, R. M. Osgood, and S. R. J. Brueck, Phys. Rev. Lett. **95**, 137404 (2005).